Effect of Heating Rate on Kinetics of High-Temperature Reactions: Mo-Si System

Suren L. Kharatyan and Hakob A. Chatilyan
Institute of Chemical Physics, National Academy of Sciences of Armenia, Yerevan, Armenia

Alexander S. Mukasyan and Dante A. Simonetti
Dept. of Chemical and Biomolecular Engineering, and Center for Molecularly Engineered Materials, University of Notre Dame, Notre Dame, IN 46556

Arvind Varma
School of Chemical Engineering, Purdue University, West Lafayette, IN 47907

DOI 10.1002/aic.10303
Published online in Wiley InterScience (www.interscience.wiley.com).

By using the Computer Assisted Electrothermography (CAE) method and taking the molybdenum-silicon system as an example, the influence of preheating rate on the kinetics of gasless reactions at high temperatures (above Si melting point, 1683 K) is studied. It is shown that an increase of heating rate V_h in the range 10–10^5 K/s, leads to a substantial increase in the rate of chemical reaction. At high heating rates ($>10^3$ K/s), the first stage of interaction involves rapid reaction due to the direct dissolution of Mo in the Si melt. Furthermore, the formation of $MoSi_2$ phase, owing both to crystallization from eutectic ($MoSi_2$-Si) melt and reaction-diffusion mechanism, is primarily responsible for the observed intensive heat release under these conditions. At lower V_h, a thin layer of Mo_5Si_3 phase formed at earlier stages (solid-solid interaction) significantly retards reaction at higher temperatures and changes the mechanism of interaction. Some methodological aspects of using the CAE technique for kinetic studies are also discussed. © 2004 American Institute of Chemical Engineers *AIChE J,* 51: 261–270, 2005
Keywords: Kinetics; molybdenum-silicon system; high-temperature reactions; heating rate; reaction mechanism

Introduction

Many engineering technologies involve chemical reactions under steady nonisothermal conditions or with preheating before reaching a stable operating temperature. It has also been reported that heating rates have an important effect on different processes, including the kinetics of chemical reactions (cf. Kharatyan et al., 1983; Seebauer et al., 1997; Pinheiro et al., 2002), phase transformation mechanisms (cf. Gordienko and Shipko, 1983), and microstructures of synthesized materials (cf. Abe, 1990; Sahay and Joshi, 2003). Thus, in general, it is well understood (cf. Koch, 1977) that under high heating rates, kinetics of interaction between the reactants may differ significantly as compared to conventional chemical kinetic laws obtained in near-isothermal conditions. However, a qualitative understanding of this fact is not sufficient to provide an adequate description of rapid high-temperature processes. The problem becomes even more complicated for the conditions, typical for various combustion and plasma syntheses (cf. Munir and Holt, 1990; Varma et al., 1998) or laser induced processes (cf. Naser et al., 1999), where rate of temperature change reaches high values, $\sim 10^4$–10^6 K/s. Indeed, in many such

Correspondence should be addressed to A. Varma at avarma@ecn.purdue.edu

cases, the observed reaction rates appear to be greater than those obtained isothermally.

The only technique known to-date that can vary the heating rate of reaction systems over a wide range (10^2–10^5 K/s) and directly measure the rate of species interaction is the so-called *electrothermography* method, which was developed originally to study oxidation and catalytic processes (cf. Grigor'ev et al., 1973; Rader and Weller, 1974). This method was also utilized previously to investigate the kinetics of gas-solid interactions (cf. Kharatyan et al. 1977; Pelekh et al., 1999). For example, it was shown that kinetics of metal (for example, Ti, Nb)-nitrogen reactions and their characteristics (for example, rate of heat release, maximum temperature, and so on) depend strongly on the preheating rate (Thiers et al., 2000; Thiers et al., 2001). It was also found that activation energy values measured under nonisothermal conditions are significantly higher than those obtained from essentially isothermal experiments. Finally, it was demonstrated recently that, by using specially prepared investigated couple (for example, W-Si) in the form of metal (W) wires clad by a thin layer of other (Si) reactant (Kharatyan et al., 1999), the same approach could also be used to investigate gasless condensed systems (Kharatyan, 1998).

By using computer assisted electrothermography (CAE) and taking the molybdenum-silicon system as an example, the goal of this work is to study the influence of preheating rate on the kinetics of gasless reactions. While some aspects of reaction mechanisms in this system have been studied by this method previously (cf. Kharatyan et al., 1995a; Kharatyan et al., 1995b), the issue of heating rate influence was not investigated. Moreover, the characteristics of the current experimental setup, allowing change of heating rate over the wide range 10 –2 $\times$ 10^5 K/s, are superior to those utilized before.

Experimental Techniques and Procedures

The clad wires were prepared as follows. The deposition of the silicon layer (δ_{Si} =0.25–5 μm thickness) on the initial Mo wire (Electronic Space Products International; 100 μm diameter, 99.97% purity) was carried out in a silane + argon gas mixture (4% SiH_4 and balance Ar) at P_{SiH4}=2 torr and T=873 K. The typical surface and cross section of Mo wire clad by Si (δ_{Si} =5 μm) are shown in Figure 1. Microstructural and phase analyses indicated that the above deposition conditions allow one to form a relatively uniform Si layer (Figures 1a and 1b) along the entire wire surface and also to avoid any interaction between Mo and Si (Figure 1c).

The details of the CAE experimental set up and procedure have been presented previously (cf. Pelekh et al., 2000). Briefly, the clad wire placed in the middle part of the reaction chamber is heated by passing electric current using a high-speed temperature controller (see Kharatyan et al., 1991; Kharatyan, 1992 for details). The experiments can be conducted in different inert gases under both static (P=10–600 torr) and steady flow conditions. The desired temperature schedule, assigned by the computer, provides control of the temperature regime, as well as continuous, automatic collection and processing of experimental data (for example, temperature of the wire, electrical power). In this studies, the heating rate (V_h) was varied from 10 to 2 · 10^5 K/s, while the investigated temperature range was 1,200 – 1,900 K.

The typical time dependences of wire temperature (T) and

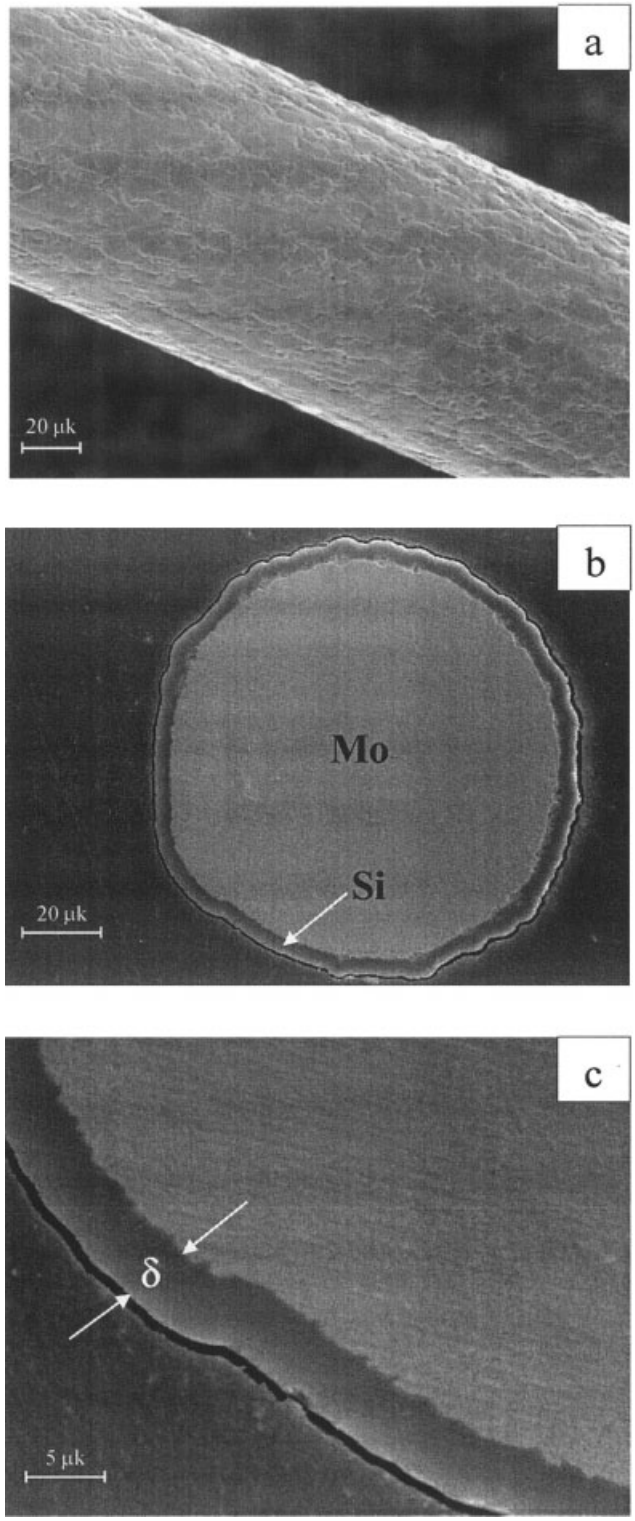

Figure 1. (a) Typical surface, and (b–c) cross section of Mo wire clad by Si.

electric power (p) obtained for different ambient atmospheres (argon and helium; $V_h \sim 10^5$ K/s) are shown in Figure 2. It can be seen that under lower heat loss conditions (argon, P=10 torr), when the wire was rapidly preheated to some reference temperature T_m, an overshooting effect (that is, wire self-

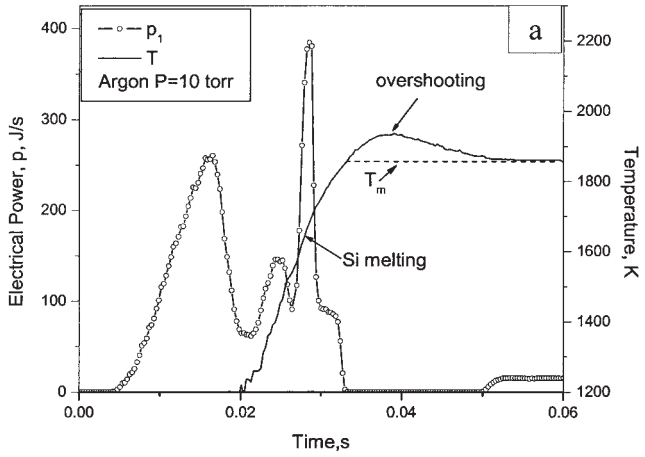

Figure 2. Typical temperature and power dependences on time: (a) Ar; (b) He (V_h=5.10^4 K/s and δ_{Si}=0.5 μm).

heating above T_m) was observed (Figure 2a; see also Pelekh et al., 1999). This phenomenon is caused by the fact that high heat release rate owing to chemical reaction cannot be compensated by heat loss and decrease of supplied electrical power, even by its full switching off, leading to the so-called *non-isothermal regime*. In higher heat loss environment (for example, helium), one may prevent the overshooting (Figure 2b), under otherwise identical V_h and T_m conditions, and the reaction proceeds at the constant reference temperature, T_m (that is, *isothermal regime*).

In both cases (isothermal and nonisothermal regimes), however, by using data on p(t) (shown in Figure 2a and 2b) and independently determined (cf. Pelekh et al., 1999 for details) heat loss rates at different temperatures h(T), one may calculate the chemical heat release function, q(t). A method for calculating this function, in the nonisothermal case, was described elsewhere (Thiers et al., 2001) and requires computation of the temperature derivative at all stages of interaction. Another approach is based on the idea of two-stage heating: (1) reaction heating as described above, followed by (2) inert heating (after the reaction is fully completed and the wire is cooled) along *identical* temperature-time schedules, which can be achieved by using the high-speed temperature controller. The latter recorded the temperature-time profile during the first stage and repeated it in the inert stage heating. Let us discuss this approach in detail.

During the first stage, with chemical reaction heat release, q(t), the wire temperature changes following the equation

$$1/2(\rho c r_0) \cdot dT/dt = q(t) + p_1(t) - h(T) \qquad (1)$$

where T - wire temperature, c - heat capacity, ρ - density, r_0 - wire radius, $p(t)$ - rate of heat generation from electric current (Joule heat), $h(T)$ - rate of heat loss, $q=\phi\ (t,T,\eta)$, - rate of chemical heat evolution and η - degree of conversion.

During the second stage, when the contribution from chemical reaction is absent (that is, q=0), but the temperature-time schedule is the same, we have

$$1/2(\rho c r_0) \cdot dT/dt = p_2(t) - h(T) \qquad (2)$$

Subtracting Eq. 2 from Eq. 1, yields a simple formula to determine the heat evolution function

$$q(t) = p_2(t) - p_1(t) \qquad (3)$$

This approach can be used for both the isothermal and nonisothermal regimes. In the former case

$$p_2(t) = h(T) = \text{constant} \qquad (4)$$

which shows how heat losses at different temperatures can be determined. A statistical analysis of experimental data revealed that the accuracy of q measurements is ~0.15 J/s, better that 1% of typical values. Note that in this work, we utilize only the isothermal regime, that is without overshooting.

Thus, by conducting experiments under different conditions and measuring $p_i(t)$, one can obtain the temperature-time dependence of the heat evolution function, q(t). Furthermore, based on a suitable model of chemical reaction and using obtained data, it is possible to extract the kinetic parameters of the reactions (cf. Pelekh et al., 1999; Kharatyan, 1998).

In addition to CAE, another *independent* approach was used to obtain the kinetics. Switching off the electric power leads to rapid cooling of the wire that quenches the reaction process. For example, for a 100 μm filament, the cooling rate varies in the range $2 \cdot 10^3$ to $5 \cdot 10^4$ K/s, depending on the nature of interaction and characteristics of the ambient gas atmosphere. Thus, by switching off the power at different stages of interaction, followed by microstructural investigation of the quenched samples, one can obtain information about the kinetics of product layer growth (cf. Thiers et al., 2000; Kharatyan and Chatilyan, 2000). In this work, the microstructures, phase and elemental compositions of cross-sections and surfaces of quenched wires were determined by different methods, including Optical (Jenavert) and Scanning Electron Microscopy (JSM 6400, JEOL; BS-300), X-Ray Diffraction (X1 Advanced Diffraction System, Scintag, Inc.) and Energy Dispersive X-Ray Microanalysis (SIGMA, Kevex).

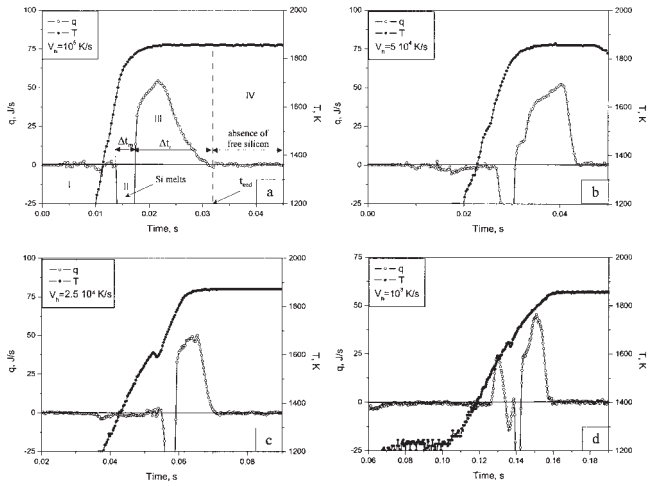

Figure 3. Temperature and instantaneous heat release as a function of time for different heating rates: (a) 10^5 K/s; (b) 5 10^4 K/s; (c) 2.5 10^4 K/s; (d) 10^3 K/s (δ_{Si}=0.5 μm).

Results

The typical plots of the heat release function (q), obtained under various heating rates (V_h= 10^3 – 10^5 K/s), thickness of the silicon layer δ_{Si}=0.5 μm and reference temperature T_m=1873 K, are shown in Figure 3. Several characteristic features can be outlined (see Figure 3a). At relatively low temperatures, during the inert preheating stage (Zone I), no heat release (q~0) was observed. The subsequent relatively narrow negative part of the heat release function (Zone II) corresponds to the melting of silicon, an endothermic process (T_{mp}=1683 K). The duration of this stage is in the range Δt_m ~0.5 – 10 ms, and depends on the heating rate and thickness of the initial Si layer, that is, higher V_h and lower δ_{Si} lead to more rapid melting. Note that under all investigated conditions, Δt_m is much smaller than the total reaction time.

The amount of heat supplied to the wire during Δt_m via electric power is not sufficient to completely melt the Si layer, thus some heat is required from the reaction itself. For example, with δ_{Si} =0.5 μm and V_h =5 10^4 K/s, the melting process takes Δt_m=1.8 ms (Figure 3b) and during this time the total electrical heat supplied is ~0.17 J, while for complete melting of 0.5 μm Si layer on a wire of length ~8 cm, under investigated heat loss conditions, one needs at least ~ 0.36 J. This result, together with the observation that within the accuracy of the experiment q=0 for T<T_{mp}(Si) (Figure 3), leads to the conclusion that under high heating rates (that is, V_h >10^4 K/s), the reaction starts at the melting point of silicon, while the contribution of solid-solid interaction is negligible.

Furthermore, the zone III (Figure 3a) with positive q is characterized by its duration, Δt_r, maximum value, q_m and cumulative heat release, $Q = \int_{\Delta t_r} q dt$. It can be seen (Figure 3a–c) that with increasing V_h, the location of Zone III shifts more within the region of constant reference temperature (T_m=1873 K). At relatively low heating rates, however, essentially complete reaction may occur before T_m is reached (Figure 3 d).

Additional experiments in which the reaction was terminated (by turning off the electrical power) at different times showed that if unreacted silicon still exists in the system, then during cooling, a plateau on the temperature profile is observed at the crystallization point, T_{mp} of silicon. Such experiments showed that if termination occurred at t>t_{end} (see Figure 3a), no such peculiarities in the temperature profile at T_{mp} (Si) were detected. Thus the last zone IV (Figure 3a) is characterized by the absence of free Si in the system.

Along with heating rate, another important parameter which influences the kinetics of interaction is thickness of the Si layer deposited on the Mo wire. The typical plots of the heat release function (q) for different δ_{Si} obtained under the same heating rate (V_h=10^3 K/s) and reference temperature (T_m=1873 K) are shown in Figure 4. It can be seen that the duration of chemical interaction depends significantly on δ_{Si}, where thicker layers correspond to longer Δt_r. Furthermore, a substantial decrease in the rate of heat release, q occurs (Figure 4 a–d).

Thus, both heating rate and silicon layer thickness influence the behavior of the heat release function q(t), by varying the location of the reaction zone III along the temperature schedule and changing reaction characteristics (for example Δt_r, q_m). Let us illustrate these aspects in detail.

Effect of heating rate

The dependences of maximum rate of heat release q_m, on V_h for wires with different δ_{Si} are shown in Figure 5a. Note that each point represents an average of at least five experiments. It may be seen that for all δ_{Si}, the maximum rate of chemical interaction increases with increasing heating rate. For example, for thin silicon layers (<2 μm), q_m increases up to 20 times when V_h changes from 10^3 K/s to 10^5 K/s. Note that wires with relatively thick δ_{Si} (>2 μm) can be preheated uniformly only with moderate heating rates, that is, V_h<10^4 K/s.

Correspondingly, the duration of reaction zone III, Δt_r, decreases monotonically with increasing V_h (see Figure 5b). At high heating rates (V_h> 10^4 K/s) and small δ_{Si} (<2 μm), the reaction time is small and in the range 10^{-3} – 10^{-1} s. Finally, cumulative heat release, $Q = \int_{\Delta t_r} q dt$, does not change with varying heating rate. An example of relative (normalized cor-

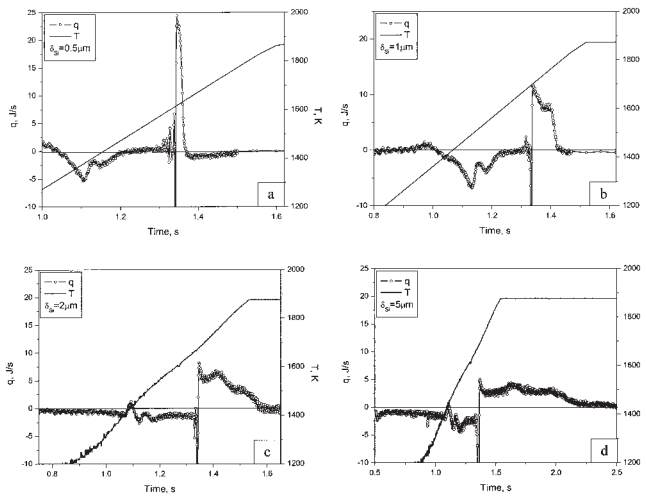

Figure 4. Temperature and instantaneous heat release as a function of time for different initial Si layer thickness: (a) 0.5 μm; (b) 1.0 μm; (c) 2.0 μm; (d) 5.0 μm (V_h=10^3 K/s).

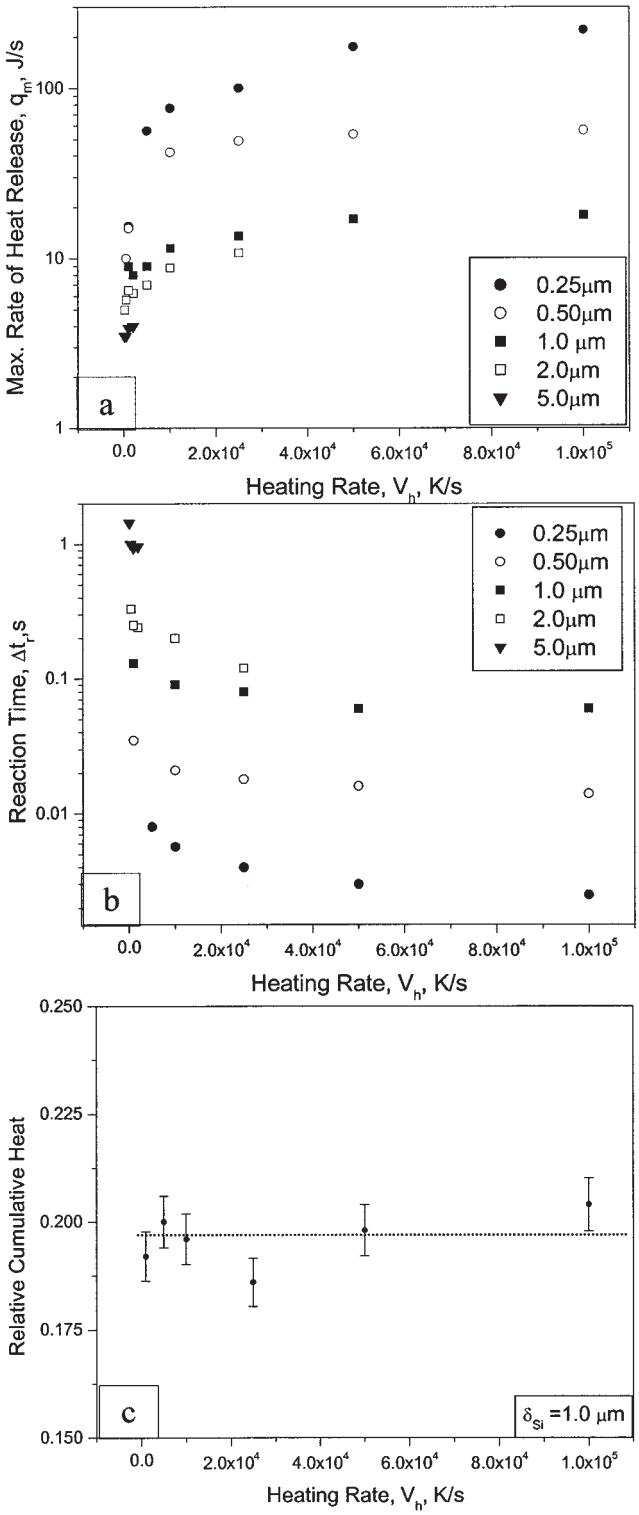

Figure 5. Influence of heating rate on: (a) maximum rate of heat release; (b) reaction duration; and (c) relative cumulative heat.

responding to the case of largest used $\delta_{Si}=5$ μm) cumulative heat for $\delta_{Si}=1$ μm as a function of V_h is shown in Figure 5c. It is reasonable that the total amount of heat released for $\delta_{Si}=1$ μm is about 5 times smaller than that for $\delta_{Si}=5$ μm.

Effect of silicon layer thickness

The dependences of reaction parameters (that is, q_m, Δt_r and Q) on δ_{Si} are presented in Figure 6a–6c. The change of silicon layer thickness strongly influences q_m (Figure 6a), and the

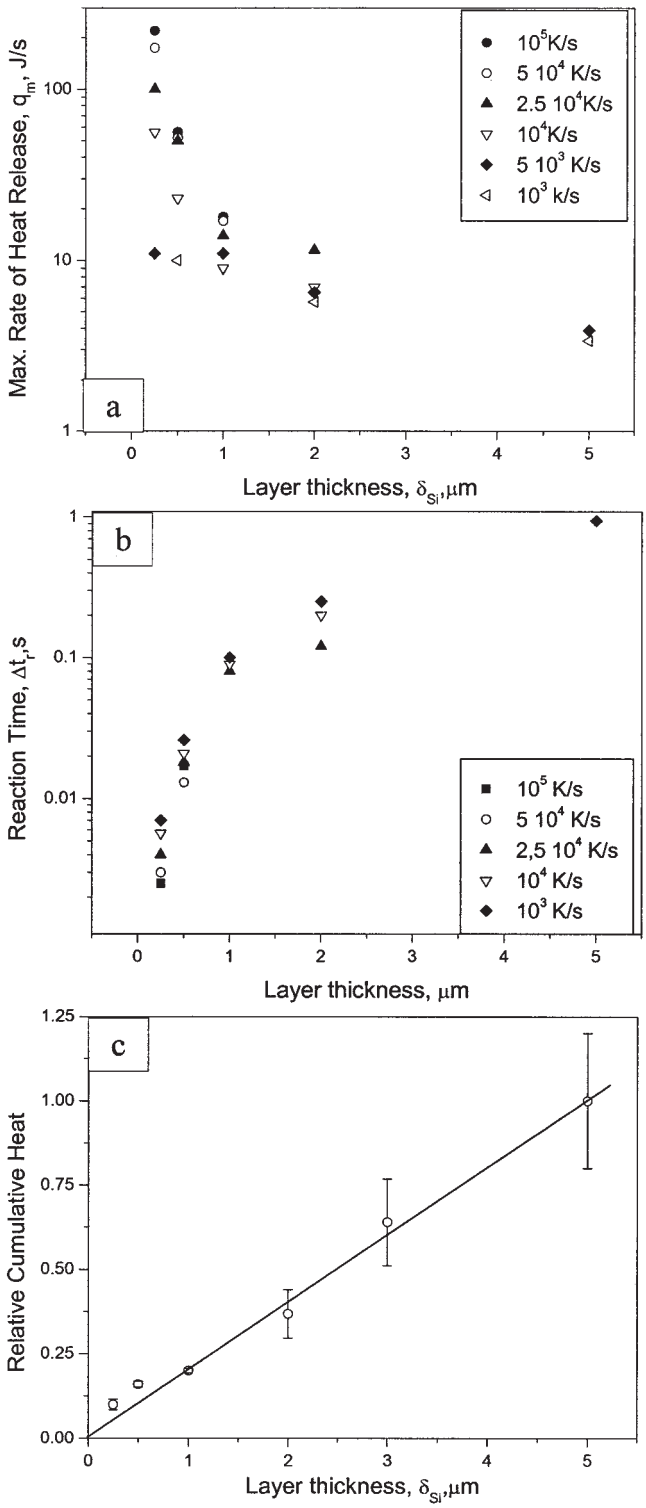

Figure 6. Influence of initial Si layer thickness on: (a) maximum rate of heat release; (b) reaction duration; and (c) relative cumulative heat.

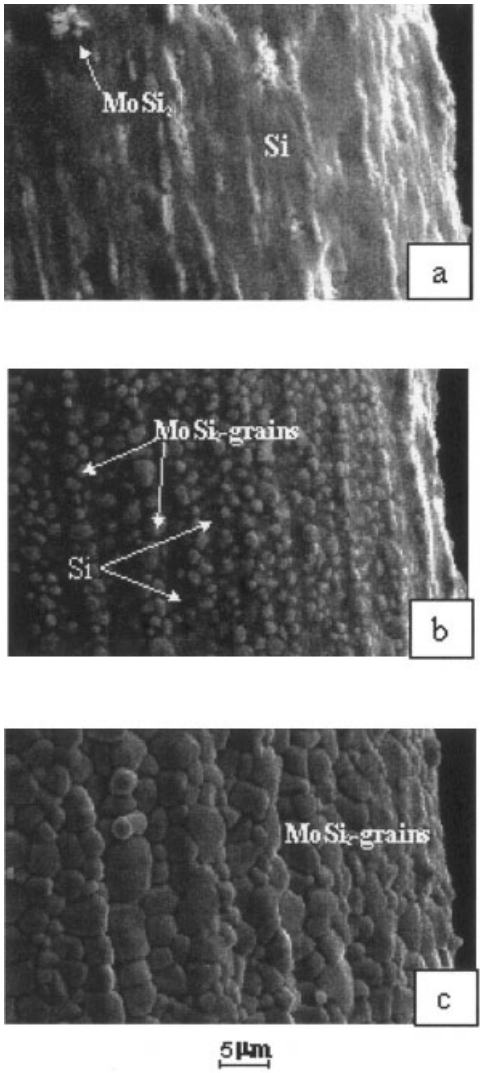

Figure 7. Typical morphological transformations in different zones: (a) zone II; (b) first stage of zone III; and (c) second stage of zone III ($V_h = 5 \times 10^4$ K/s, $\delta_{Si} = 2$ μm).

duration of the reaction zone III, Δt_r (Figure 6b). For example, an increase of δ_{Si} from 0.5 to 5 μm (with V_h in the range 10^3 to 10^4 K/s) results in three-fold reduction of q_m (Figure 6a), despite a higher average reaction temperature for systems with higher thickness (compare Figure 4a–d). Note that the part of the q(t) curve with essentially constant reaction rate is relatively long for thick Si layers (Figure 4c,d) and practically disappears for $\delta_{Si} < 1$ μm (Figure 4a,b). Moreover, the number of characteristic subzones with different constant q increases with increasing δ_{Si}, implying complexity of the chemical interaction.

Finally, as expected, the cumulative heat release, Q, increases essentially linearly with increasing δ_{Si} (Figure 6c). Indeed, the total amount of heat generated during the reaction is proportional to mass of the limiting reactant (that is, Si), which, for relatively small δ_{Si} (0.25−5 μm) as compared to the Mo wire diameter (100 μm), depends linearly on δ_{Si}.

Microstructural Transformations

The typical microstructure of the silicon layer surface after its low-temperature deposition on the Mo wire, is shown in Figure 1. Analysis shows that the surface consists of Si grains with size of about the layer thickness. As described in the "Experimental Techniques and Procedures" section, by quenching wires at different stages of interaction (see Figure 3a), one can obtain a dynamic picture of the structural and phase transformations that occur during heat treatment of clad wires. Typical sequences of such morphological transformations are presented in Figures 7a–7c and Figure 8a-8f 8 for $\delta_{Si} = 2$ and 5 μm, respectively.

It can be seen that upon reaching $T_{mp.}$ (1683 K), rapid melting of silicon occurs which destroys the initial grain structures of silicon layer (Figure 7a and 8a). Furthermore, both product grain formation and rapid growth take place (Figure 7b and 8b–c), however, EDX analysis also shows the presence of pure Si on the surface. Finally, when all silicon reacts, corresponding to the end of the reaction zone III (see Figure 3a), grain growth rate sharply decreases (Figure 8d–8f). Note that the grain size of the "primary" products does not depend on thickness of the silicon layer (compare Figure 7b and 8a), but at the end of the reaction zone this size is larger for samples with higher initial δ_{Si} (compare Figure 7c and 8f).

The evolution of structural transformations is illustrated by the micrograph sequence of the sample cross-sections, quenched at different times (see Figure 9), using as an example the initial clad wires with $\delta_{Si} = 5$ μm. Immediately upon reaching the silicon melting point, one can observe the formation of $MoSi_2$ grains in the volume of the silicon matrix (Figure 9a). At

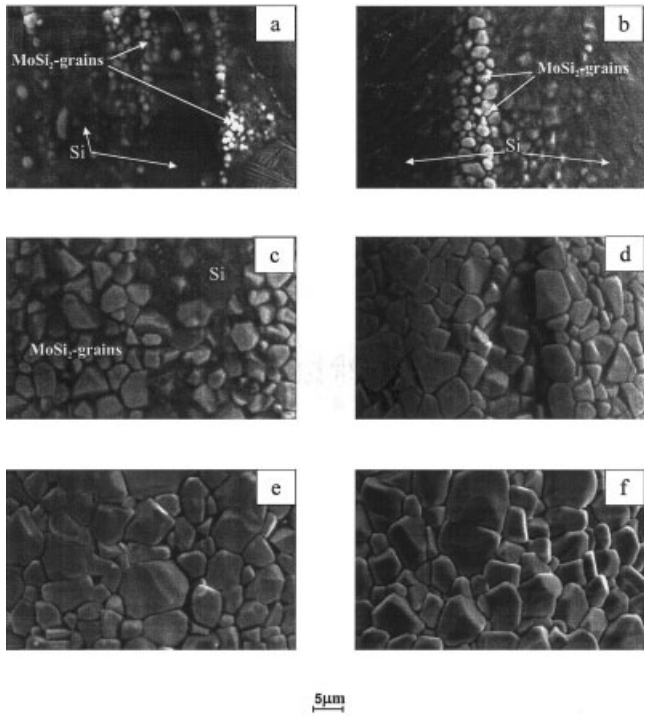

Figure 8. Typical morphological transformation in different zones (a) zone II; (b) first stage of zone III; (c) second stage of zone III; (d–f) along zone IV ($V_h = 5 \times 10^4$ K/s, $\delta_{Si} = 5$ μm).

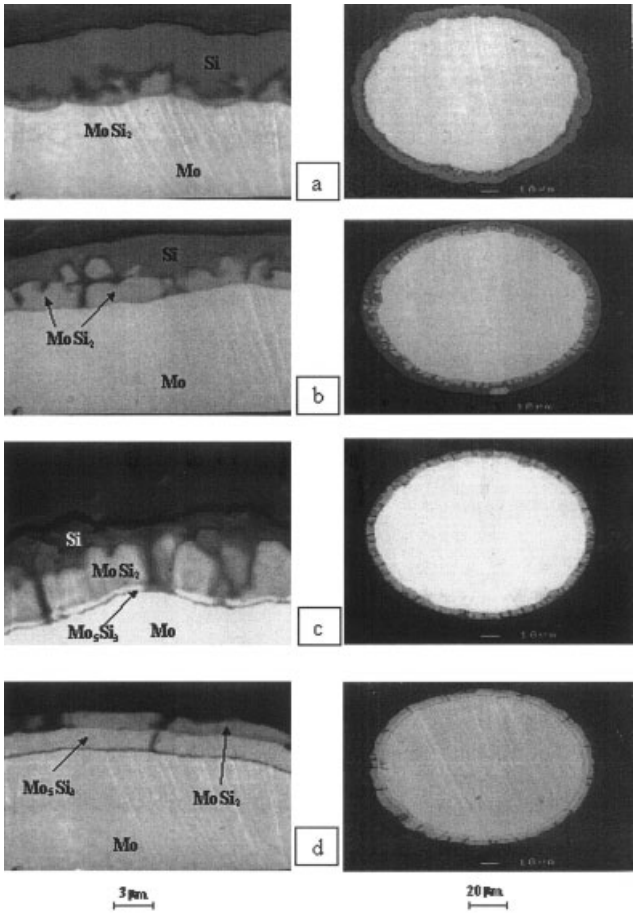

Figure 9. Micrographs of the sample cross-sections, quenched at different times of interaction: (a) zone II; (b) first stage of zone III; (c) second stage of zone III; and (d) zone IV (V_h =5 × 10^4 K/s, δ_{Si}=5 μm).

this stage, the grains do not form a continuous layer around the Mo wire, but are mainly located close to the metal surface (Figure 9b).

Soon thereafter, a very thin (0.1–0.3 μm) compact layer of another product (Mo_5Si_3) with a higher concentration of Mo, which separates the metal from the melt (Figure 9c), could be detected (COMPO mode). Simultaneously, more $MoSi_2$ grains appear in the melt, which form a continuous layer around the Mo core. Finally, after complete Si consumption (end of the reaction zone), redistribution between the $MoSi_2$ and Mo_5Si_3 layers occurs, where the latter grows at the expense of the former (Figure 9d).

Phase transformations

To confirm the above conclusions made based on SEM and EDX analyses, additional studies of quenched samples were made by utilizing the XRD technique. For this purpose, clad wires with δ_{Si} =2 μm, heated under similar conditions (V_h~5 10^4 K/s and T_m =1873 K), were quenched after different process durations (that is, 50, 100 and 300 ms). The wires were then cut into pieces of ~1cm length, which were used to completely cover areas ~1cm^2 in size for XRD analysis.

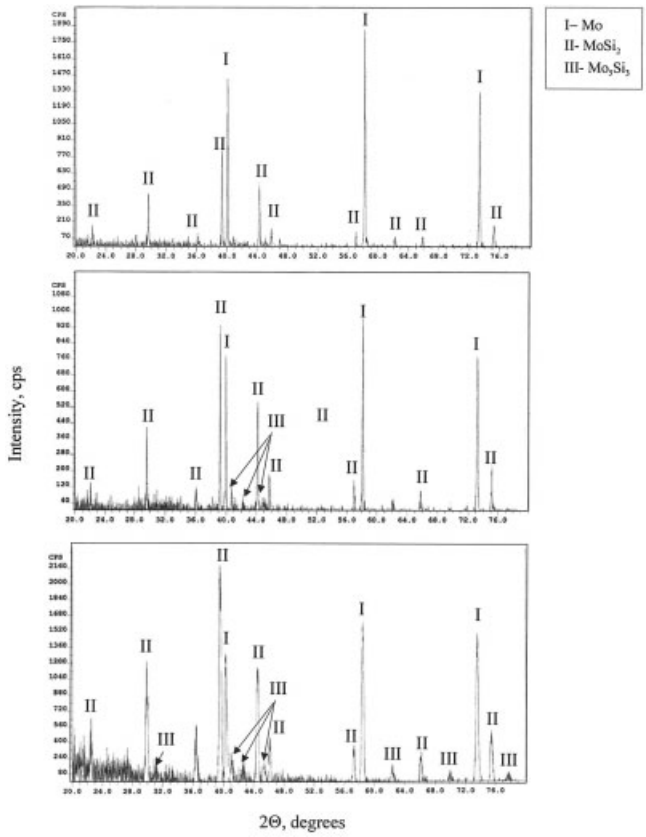

Figure 10. Characteristic XRD patterns for samples quenched in different zones: (a) first stage of zone III; (b) second stage of zone III; (c) zone IV (V_h =5 × 10^4 K/s, δ_{Si}=2 μm).

Typical diffraction patterns obtained after different heat treatments are shown in Figure 10a–10c. At the used heating rate, it takes ~30 ms to preheat wire to silicon melting point at which, as discussed earlier, rapid reaction initiates and under these conditions, typical reaction time is ~ 100 ms (see Figure

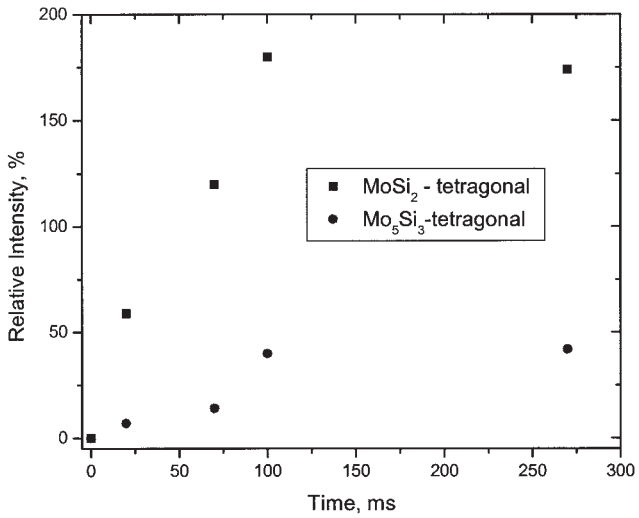

Figure 11. Kinetics of phase formation in Mo-Si system (V_h =5 × 10^4 K/s, δ_{Si}=2 μm).

6). Thus, patterns shown in Figure 10a–10c correspond to wires which were exposed to temperature 1873 K for 20, 70 and 270 ms. The first two of these correspond to zone III, while the last one represents the product in zone IV.

After 20 ms of reaction (Figure 10a), peaks of Mo and tetragonal $MoSi_2$ phases can be easily detected. The ratio between $MoSi_2$ and Mo peaks increases substantially after 70ms of reaction (Figure 10 b), indicating growth of $MoSi_2$ fraction. Simultaneously, peaks related to the Mo_5Si_3 phase also become evident. The final product of reaction (Figure 10 c) contains all three phases (that is, Mo, $MoSi_2$ and Mo_5Si_3), however, Mo peaks are wider and shifted slightly to larger diffraction angles (compare Figure 10 a and c), indicating the formation of Si solid solution in Mo.

The kinetics of phase formation in terms of the relative peak intensities (normalized to the intensity of Mo peak at $2\theta=40.105°$) is shown in Figure 11. It can be seen that the intensity of $MoSi_2$ peaks increases continuously up to 100ms of reaction (end of the zone III) and then decreases slowly. Thus, formation of this phase is *primarily* responsible for the intensive heat release in this stage. The role and sequence of Mo_5Si_3 phase formation is still unclear but, in any case, its contribution to the total heat release is relatively small.

Discussion

We now discuss the influence of experimental parameters (V_h and δ_{Si}) on the kinetics of interaction in the Mo-Si system. Furthermore, we develop the reaction mechanism under the high heating rate and temperature conditions typically encountered in processes such as combustion synthesis of advanced materials.

Influence of heating rate and Si layer thickness

As shown earler, increasing V_h shifts the heat release function to the high temperature region, along with substantial increase of q_m (Figure 3 and 5). There are two reasons for the observed effects. First, at higher V_h and constant T_m, the reaction proceeds at higher *average* temperature. Second, negligible solid-solid reaction occurs during preheating stage at high V_h, minimizing the formation of diffusion layers that retard chemical reaction rates at T_m.

Increase of δ_{Si} substantially widens the reaction zone III and shifts it toward higher temperatures (Figure 4 and 6). In addition, it simultaneously leads to a decrease in the maximum heat release rate, q_m (Figure 6a). These effects may be explained as follows. For smaller δ_{Si}, the Si melt can be rapidly and *uniformly* saturated by Mo in the first stage of interaction in zone III. Thus, crystallization of $MoSi_2$ occurs rapidly and essentially simultaneously in the entire bulk of the melt. For larger δ_{Si}, formation of $MoSi_2$ grains near the Mo surface (Figure 9b,c) retards Mo-Si interaction, thus, widening reaction zone III. Also, thicker Si layer, especially its outer periphery, being inert during the first stage of interaction, increases heat capacity of the system and, hence, decreases q_m. However, an accurate kinetic model of Mo dissolution in Si under the investigated conditions needs to be developed to prove this hypothesis, and is currently in progress. The obtained data also allow one to construct the diagram of operating regimes, depending on the values of heating rate and silicon layer thickness (Figure 12). It may be seen that for each δ_{Si}, a critical V_h exists above which (Region I) the interaction proceeds essentially at T_m (that is, isothermal conditions). However, for lower V_h values (Region III), the heat release ends prior to achieving the reference temperature, T_m. In this case, change of T_m does not influence the interaction parameters: Δt_m, q_m and Q. Finally, in between, an intermediate region II exists, where the reaction occurs partially in both isothermal and nonisothermal conditions. It is evident that operation in region I is desirable for extracting the intrinsic kinetics. Thus, this work contributes not only toward fundamentals of interaction in gasless systems, but also to methodological aspects of using the CAE technique for kinetic studies.

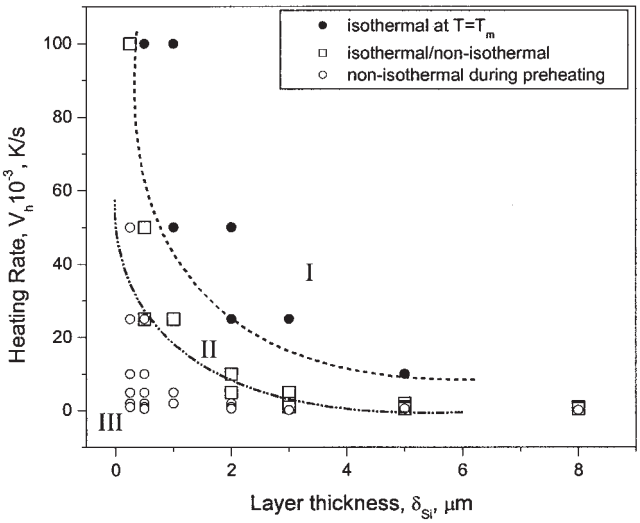

Figure 12. Parametric V_h-δ_{Si} diagram of operating regimes.

Reaction mechanism

On the basis obtained results on typical heat release functions (Figure 3 and 4), as well as microstructural observations (Figure 7–11), the following mechanism of interaction in the Mo-Si system can be suggested. Over the wide range of investigated parameters (see notes about exceptions at the end of this section), the reaction starts at the melting point of silicon $T_{mp.}(Si)=1683$ K. Since, owing to high heating rates, the product layer has no time to form as a result of solid-solid reaction, pure contact between solid Mo and liquid silicon exists at the very first moment of melting. Thus, the *first stage* of interaction involves rapid reaction due to Mo *dissolution* in Si.

This conclusion is supported by different arguments. First, some $MoSi_2$ grains observed in the quenched samples formed in the melt volume without connection with the metal surface. Second, while located predominantly near the Mo surface, these grains do not form a continuous product layer. Furthermore, the grain size of "primary" products remains essentially constant for all δ_{Si}. Third, the Mo-Si phase diagram shows that up to ~20 wt % Mo may dissolve in Si at the investigated temperature T_m =1873 K (Samsonov and Vinitskii, 1980). Finally, Mo-rich phases do not form in this stage, as observed for lower heating rate conditions. Thus all of the earlier con-

siderations suggest that the small (<1 μm) grains of $MoSi_2$ phase observed (Figure 7a and 8a and 8b) in the quenched samples formed during cooling due to crystallization from the melt.

The *second stage* of interaction begins when the concentration of Mo in the liquid reaches saturation value (that is, ~20 wt %), and $MoSi_2$ crystallites form in the melt at high-temperatures. The $MoSi_2$ grains accumulate around the Mo core, forming a relatively compact layer (Figure 9b), and the process of $MoSi_2$ crystallite nucleation is accompanied by their growth. It is important to note that grain growth proceeds rapidly up to the complete consumption of silicon (Figure 7a–c, Figure 8a–d). Because the reaction duration increases with Si layer thickness (Figure 6b), the average final size of $MoSi_2$ crystallites depends on δ_{Si}, that is, for larger δ_{Si}, larger $MoSi_2$ crystallites are formed (compare Figure 7c and 8f).

Furthermore, during this stage of interaction, a thin Mo_5Si_3 layer was also detected (Figure 9c and 10b). Once formed, the thickness of this layer changes little during zone III, while $MoSi_2$ grains continue to grow. Since the Mo diffusion coefficient in all molybdenum silicides is significantly lower than for Si (Yoon et al., 2002; Byun et al., 2002), this means that the Mo_5Si_3 layer dissolves in the melt (from the liquid Si side) and continues to grow owing to the Si diffusion through the layer and reaction on the opposite Mo-rich side. The formation and continued presence of this layer during the reaction process may explain the complex features of the heat evolution function q (Figure 3 and 4). It may be expected that high values of q at the beginning (first stage) of region III arise from pure dissolution of Mo in the Si melt, while subsequent (second stage) lower q values correspond to the reaction progress after Mo_5Si_3 layer forms.

Finally, after complete consumption of silicon, two compact silicide layers (that is, $MoSi_2$ and Mo_5Si_3) exist (Figure 9c and 10c), and the q values become negligible. At this stage, only growth of the Mo_5Si_3 layer at the expense of the $MoSi_2$ phase takes place (zone IV, Figure 3a and Figure 9d). Note that in zone IV, the rate of Mo_5Si_3 layer growth is about 10 times larger as compared to zone III when Si is present. The reason for such behavior is the comparatively high diffusivity of silicon in the $MoSi_2$ layer, as compared to Mo_5Si_3 (Barlett et al., 1964).

Finally, under relatively low heating rate conditions (Figure 3d), heat evolution owing to chemical interaction was observed for temperatures below the Si melting point (1683 K). Due to the extremely short duration of this stage, it is difficult to identify the product by using quenching experiments. However, traces of Mo_5Si_3 phase, as a result of solid-solid interaction, were detected by EDX analysis on quenched samples preheated to T_{mp}. (Si) with $V_h = 10^3$ K/s. The formation of this layer retards interaction between Si and Mo, decreasing q_m and prolonging Δt_r. Thus, the heating rate not only influences kinetic parameters but also may even change the qualitative reaction mechanism.

Concluding Remarks

It is demonstrated that the computer assisted electrothermography (CAE) method is a powerful tool to investigate the initial stages of high-temperature chemical interactions for "pure" diffusion couples, that is, without prior formation of any diffusion layers. It is important that since CAE systems are of microscopic length scale, the kinetic data obtained could be directly applied to describe the behavior of heterogeneous reactions, for example during combustion of different powder mixtures widely used for the synthesis of advanced materials.

It is also shown that heating rate (V_h) influences the reaction kinetics in gasless systems, that is, increasing of V_h leads to higher rate of chemical reaction. The latter explains why extremely rapid reaction rates are typically observed in high-temperature gradient combustion waves, as they propagate along heterogeneous gasless reaction media.

On the basis of the suggested mechanism of interaction in the Mo-Si system, we are currently developing a mathematical model that will allow one to extract the intrinsic kinetic parameters from the obtained experimental data.

Acknowledgments

We gratefully acknowledge financial support from NSF (grant CTS-02022765) and NFSAT/CRDF (Award CH 121-02/12045).

Literature Cited

Abe, O., "Sintering of Y_2O_3 and Al_2O_3-doped Si_3N_4," *J Mat. Sci*., **25**, 4018 (1990).

Bartlett, R. W., P. R. Gage, and P. A. Larsen. "Growth Kinetics of Intermediate Silicides in the $MoSi_2$/Mo and WSi_2/W Systems," *Trans. Metall. Soc. AIME.*, **230**, 1528 (1964).

Byun, J., J. Yoon, G. Kim, J. Kim, and C. Choi. "Study on Reaction and Diffusion in the Mo-Si System by ZrO2 Marker Experiments," *Script. Mater.*, **46,** 537 (2002).

Gordienko, A. G., and A. A. Shipko, *Structural and Phase Transitions of Titanium Alloys at Rapid Heating* (in Russian), Nauka I Tehnika: Minsk (1983).

Grigor'ev, Y. M., Y. A. Gal'chenko, and A. G., Merzhanov, "Investigation of the Rate of the High-Temperature Reaction between Aluminum and Oxygen using the Ignition Method," *Combust. Explos. Shock Waves*, **9**, 162 (1973).

Kharatyan, S. L., Y. M. Grigor'ev, and A. G. Merzhanov, "Kinetics of Heat Release during High-Temperature Titanium Nitration," *Izv. Akad. Nauk USSR, Ser. Metals*, **10**, 178 (1977).

Kharatyan, S. L., A. B. Harutunyan, and A. G. Merzhanov, "Diffusive Kinetics of Interaction in Multiphase Binary Systems," [in Russian], *Khimicheskaya Fizika*, **10,** 1399 (1983).

Kharatyan, S. L., G. H. Voskerchyan, and A. G. Merzhanov. "New Method for Study of the Mechanism and Wave Structure of SHS," *Dokl. Akad. Nauk USSR*, **316,** 415 (1991).

Kharatyan, S. L., "Kinetic Modeling of Combustion Waves in SHS Systems," *Inter. J. SHS,* **1**, 536 (1992).

Kharatyan, S. L., H. A. Chatilyan, and A. G. Dorunts, "Kinetics of Molybdenum Siliconizating," I. Below the Silicon Melting Point," *Chem. Phys. Report*, **14**, 735 (1995a).

Kharatyan, S. L., H. A. Chatilyan, and A. G. Dorunts, "Kinetics of Molybdenum Siliconizating," I. Above the Silicon Melting Point", *Chem. Phys. Report*, **14**, 743 (1995b).

Kharatyan, S. L., "Kinetic Modeling of Tantalum Carbidization in Combustion Wave", *Int. J. SHS*, **7**, 439 (1998).

Kharatyan, S.L., and H. A. Chatilyan, "Non-Isothermal Kinetics and Mechanism of Interaction of Tungsten with Silicon in Gasless Combustion Wave," *Int. J. SHS*, **8**, 31 (1999).

Kharatyan, S. L., and H. A. Chatilyan, "Regularities of Heat Release During Tungsten Siliconizing in a Gasless Combustion Wave," *Combust. Explo. Shock Waves*, **36**, 342 (2000).

E. Koch, *Non-Isothermal Reaction Analysis*, Academic Press, New York (1977).

Z. A. Munir, and J. B. Holt, ed., *Combustion and Plasma Synthesis of High-Temperature Materials*, VCH Publishers, Inc., New York, (1990).

Naser, J., H. Ferkel, W. Reihemann, and B. L. Mordike, "Laser-Induced Synthesis of Nanoscaled Tin Oxide-based Powder Mixtures," *Lasers in Engineering,* **9**, 195 (1999).

Pelekh, A., A. S. Mukasyan, and A. Varma, "Kinetics of Rapid High-Temperature Reactions: Titanium-Nitrogen System," *Ind. & Eng. Chem. Res*., **38**, 793 (1999).
Pelekh, A., Mukasyan, A. S., and A. Varma, "Electrothermography Apparatus for Kinetics of Rapid High-Temperature Reactions," *Rev. Sci. Instrum.*,**71 (1)**, 220 (2000).
Pinheiro, G. F. M., V. L. Lourenco, and K. Iha, "Influence of the Heating Rate in the Thermal Decomposition of HMX," *J. Therm. Anal. Calorimet*., **67**, 445 (2002).
Rader, C. G., and S. W. Weller,., "Ignition of Catalytic Wires: Kinetic Parameter Determination by the Heated-Wire Technique," *AIChE J*., **20**, 515 (1974).
Sahay, S., and B. Joshi, "Heating Rate Effects during Non-Isothermal Annealing of AIK Steel," *J. Mat. Eng. Perform.,* **12,** 157 (2003).
Samsonov, G. V., and I. M. Vinitskii, *Handbook of Refractory Compounds*, IFI/Plenum, New York (1980).
Seebauer, V., J. Petek, and G. Staudinger, "Effects of Particle Size, Heating Rate and Pressure on Measurement of Pyrolysis Kinetics by Thermogravimetric Analysis," *Fuel*, **76,** 1277 (1997).
Thiers, L., B. Leitenberger, A. S. Mukasyan, and A. Varma, "Influence of Preheating Rate on Kinetics of High-Temperature Gas-Solid Reactions," *AIChE J.,* **46,** 2518 (2000).
Thiers, L., A. S. Mukasyan, A. Pelekh, and A. Varma, "Kinetics of High-Temperature Reaction in Titanium-Nitrogen System: Non-Isothermal Conditions," *Chem. Eng. J.,* **82**, 303 (2001).
Varma, A., A. S. Rogachev, A. S., Mukasyan, and S. Hwang, "Combustion Synthesis of Advanced Materials: Principles and Applications," *Advances in Chem. Eng.*, **24**, 79 (1998).
Yoon, J., J. Byun, G. Kim, J. Kim, and C. Choi. "Multilayer Diffusional Growth in Silicon-Molybdenum Interactions," *Thin Solid Films*, **405**, 170 (2002).

Manuscript received Aug. 4, 2003, and revision received May 21, 2004.